Research Paper

Probabilistic Seismic Demand Assessment of Chevron Brace Steel Moment Frames with TADAS Damper

Hadi Sedaghatnezhad[1], Ahmadali Fallah[2*] and Mohamadreza Mosalman Yazdi[2]

1. Ph.D. Candidate, Department of Civil Engineering, Maybod Branch, Islamic Azad University, Maybod, Iran
2. Assistant Professor, Department of Civil Engineering, Maybod Branch, Islamic Azad University, Maybod, Iran,
*Corresponding Author; email: ahmadalifallah.eng1401@gmail.com

ABSTRACT

In this paper, the seismic performance of concentrically braced steel frames equipped with TADAS damper has been investigated with emphasis on earthquake uncertainties. For this purpose, first, relying on laboratory and finite element results, the behavioral model of TADAS damper has been presented and verified. Afterwards, adopting the TADAS damper connection model and non-linear conditions, two-dimensional moment frames were used with 4 m floor height and length of different spans in FEMA P695 regulations and also 10 records were used that have the highest PGA in FEMA P695. To reflect the uncertainties associated with earthquakes, the incremental dynamic analysis procedure was performed. The procedure outcomes, which consist of more than 2500 nonlinear dynamic analyzes. Thus, nonlinear dynamic analysis of the studied structures was performed and the results of these analyzes were used to estimate the performance of the frames in terms such "limit-state frequencies", "seismic demand hazard curve". The results may be used in comparing the studied structures with other similar structures and also as a crisis to the prescriptions issued by design guidelines for the structures under consideration and reveal the difference between the collapse behaviors of low and high-rise structures

1. Introduction

Different methods have been tested and studied for designing high efficient buildings against earthquakes. In conventional methods, the building shows resistance against earthquake using a combination of hardness, ductility, as well as energy dissipation. Steel moment frame is always used as a desirable system in construction because of its good ductility and high energy absorption capacity during earthquakes, but its main weakness is high displacement and low hardness. As a result, the restraint system was introduced to compensate for this weakness. The approach of earthquake en-gineering in recent years has been to optimize the dynamic properties of the structure in order to reduce the force applied to the structure and guide the non-elastic deformation to the predetermined locations. Hence, some methods were invented to increase the natural period of the structure, such as seismic separation devices, and some other methods were developed to increase the damping ratio, such as yielding dampers (Winters & Constaninou, 1993). The bracing members in the concentric braced system are responsible for providing rigidity, ductility and resistance. The

non-elastic buckling of the brace and the tensile joints created in the brace as the main factors of energy absorption result in the development of plastic joints in other parts of the structure (Khatib et al., 1988), which perform well with yielding dampers. The yielding steel dampers are based on energy dissipation in the structure developed through plastic deformation. This type of damper was first used in New Zealand and Japan and later to strengthen structures in the United States (Chan et al., 2015).

In order to use buildings immediately after an earthquake, it is preferred to limit damage to energy-absorbing elements that have good hysterical properties so that it is not transferred to the main structural elements (beam and column). This factor has caused the use of a source of depreciation other than beam columns in structures to become common (Saffari et al., 2013). One of the most popular mechanisms for energy dissipation in structures is the use of metal yield. Research has been done on inactive metal depreciation devices over the past three decades, and many metal dampers have been proposed and used (Chan & Albermani, 2008). Tsai et al. (1993) recommended design for the use of TADAS dampers, and these dampers were examined in a laboratory in a two-story structure under seismic load. They examined the seismic behavior of these dampers.

In a laboratory study by Wada et al. (1997) performed on a steel slit damper, they assembled the slit damper at the location of the bracket mounted on the beam in the main frame. Their results showed that steel slit damper has had a stable hysteresis loop and tend to harden after yielding (Lee et al., 2017). In 2008, Benavent-Climent (2008) used a steel slit damper at the connection of the cross braces to prevent buckling of the cross braces and absorbing seismic energy. In this study, the maximum energy absorption capacity was investigated by a steel slit damper under shear forces. They predicted the R-displacement curve under uniform load using the three-line model. The results of their research showed that the steel slit damper has had stable hysteresis behavior under shear forces. Seismic design was used with a com-bination of hardness and flexibility in reinforced concrete structures. For this purpose, the columns

were slim and designed with heavy reinforcement to be ductile, and energy dissipation devices and reinforced concrete walls which attached slit dampers to the frame were built with great difficulty.

In 2009, Oh et al. (2009) examined these types of steel slit dampers in connections, and investigated the energy absorption and hysteresis behavior of these connections under seismic loads and concluded that the connections attached to the steel slit dampers have more ductility. Also in 2019, Bayat & Shekasteband (2019) have examined the slit connectors in T-shaped connections and concluded that the energy absorption of these T-shaped connections with slit connectors is higher than their previous models. In 2010, other researchers studied the optimal seismic design of a steel moment frame with metal or yielding dampers with a bracing system, which includes damper optimization variables such as damper height, damper type, yield strength, and hardness. They have used the genetic algorithm to solve the problem of optimization and used SRSS of relative displacement of the floors or acceleration of the floor to evaluate the response of the optimized structure with the damper. In the pre- and post-improvement modes, with the optimal increase of dampers, it has been shown that after the optimal design, the parameters mentioned above decrease and the distribution of floor acceleration and relative displacement of floors becomes more uniform (Apostolakis & Dargush, 2010). Karavasili et al. (2012) examined the hysteretic model based on the characteristics of the SSD damper and existing defects and provided modifying parameters to improve the behavior of the hysteretic cycle. Xu et al. (2011) studied the new form of these types of dampers and examined the parabolic shape of this type of damper and stated that it absorbs more energy from the slit damper compared to the shapes previously suggested in the articles. Teruna et al. (2015) tried to increase energy absorption in a study by changing the geometry of steel slit dampers.

Lee et al. (2016) have proposed new strips for steel slit dampers that increase the energy absorption of these dampers. Also, Keykhosravi & Aghayari (2017) examined the behavior factor (R) of reinforced concrete frames with chevron

brace equipped with a steel slit damper in an article and have studied these dampers in concrete structures. In 2017, lee et al. (2017) studied the steel slit dampers and examined the energy absorption of these dampers in an incremental dynamic analysis and also studied the fragility curves of these dampers. In 2018, Ahmadi Amiri et al. (2018) had new metal yielding dampers called BSD with better seismic performance than the previous model of split steel dampers. Also in 2020, in another research, they optimized block steel damper (BSD) and these researchers studied the geometric changes in dampers, increased energy absorption, and stabilized the hysteretic behavior of these dampers (Katal Mohseni et al., 2020). Also, several researchers have studied the seismic demand of different dampers. Among them, Sourav Gur et al can be mentioned, who studied and compa0red yielding metal dampers and dampers with memory alloys, they cited that smart materials such as memory alloys have unique properties which can decrease and mitigate the risks of earthquake in a built environment (Gur et al., 2019). After comparing steel yielding damper with damper having memory alloy, they stated that earth movements and different types of modelling uncertainty in structural parameters have been done under different levels, and it can be said that both proposed dampers in this article have reduced the seismic damage of the building and also makes the damper equipped with a memory alloy perform better at the levels of the safety system. In another study, the performance of steel slit dampers was evaluated and the effect of uncertainty of the parameters of steel slit dampers on the seismic demand in the building equipped with these dampers was determined using a possible approach. In the mentioned study, two steel buildings were evaluated, which were designed in accordance with the European standard design code in OpenSEES software, and also hazard and fragility curves were plotted (Wijaya et al., 2019). In another study, Katal Mohseni et al. (2020), studied the effect of geometric parameters on energy absorption of steel structural elements and concluded that by changing the geometric parameters, structural performance and safety levels can be improved.

These TADAS dampers can be used at different levels according to the design requirements of the structures, and regarding the construction and execution costs, it can be said that because of the configuration of these dampers, the construction costs are lower and their design and implementation is easier than other dampers. Therefore, in this paper, the seismic demand of these dampers in the structure with different classes of seismic flat loads has been investigated using incremental dynamic analysis.

2. Simulation Assumptions and Verification

To ensure the accuracy of the results of this study, it is necessary to validate the results, and to fulfill the validation, the article by Tsai et al. (1993) has been used. In this study, Tsai et al. (1993) studied the effect of TADAS steel damper on the structure under high seismic risk using a shaking table test on a two-story steel frame. This two-story steel frame has a span of 4 m and the height of the first floor is 2710 mm and the height of the second floor is 5220 mm. All of the steels used in this two-story frame are made of ASTM A36 steel. It should be mentioned that Sample No. 2 in Tsai et al. (1993) study has been used to validate this study. They used several seismic records with different intensities. As part of their laboratory research, the frame equipped with TADAS steel damper was put under the north and south components of El Centro 1940 earthquake scaled to maximum ground acceleration or PGA = 312 cm /s². OpenSEES software was used to simulate this study, and the numerical and laboratory results were well matched. To validate this article, an attempt has been made to carefully examine all the factors affecting the response of the damper time displacement diagram, such as defined materials, loading, boundary conditions, etc. in order to reach the closest possible answer in Figure (1).

3. Modelling

Incremental dynamic analysis is a nonlinear dynamic analysis that can be used to determine the amount of damage caused by the severity of an earthquake. In this method, the accelerogram of past earthquakes are scaled to cover the behavior of the structure from the linear elastic state to the phase of collapse of the structure. In other words,
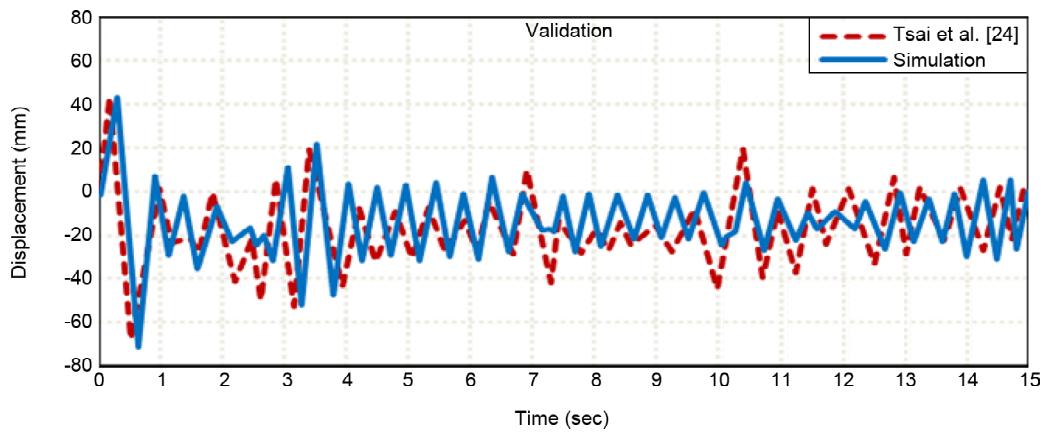
Figure 1. The difference between simulated and experimental graphs of Tsai et al. (1993).

in this method, which was also developed to evaluate the effect of uncertainty in earthquakes in evaluating the seismic response of structures; a suitable number of records must be used to take into account the uncertainty in the frequency and spectral shape of earthquakes. Each earthquake record is then scaled to cover a range of seismic intensities as well as structural behavior, from elastic to destructive limit. Finally, by using the results of this analysis and determining the limit state of the desired collapse and summarizing and interpreting the resulting curves, it is possible to study the performance and behavior of the structure under different earthquake records and also assess the probability of seismic demand of structures.

In this study, three types of structures of 3, 6 and 9 floors and 9.1 span with eccentrically braced steel frames with TADAS damper were investigated, which have been simulated in OpenSEES software. in Figure (2) and Table (1). Initially, they were affected by 10 earthquake records using the FEMA P695 Regulation (2009) and an incremental dynamic analysis was performed on them. The IDA curves are then plotted and summarized for each frame. Finally, by determining

the limit states associated with the performance levels of the structures, the capacity of S_a (the base acceleration of design) of the structures and the return period of the earthquakes are calculated with the occurrence of limit states and fragility curves are presented for brace frames with TADAS damper and also ST-37 steel is used as steel materials with a density of 7850 kg/m³, Poisson ratio of 0.30, yielding stress of 241 MPa, failure stress of 400 MPa, and elasticity module of 200 GPa.

For modeling of columns the fiber method was used and for its element nonlinear beam-column method was used. In this research, uniaxial materials Steel02 with isotropic hardening were used. For the beam, the nonlinear beam-column element whose steel stress-strain diagram is used to consider the axial stiffness and nonlinear materials with 2% hardening are used to consider the nonlinear bending behavior. Besides, bracing is modeled with Corotational Truss element. Corotational Truss element consists of uniaxial Material Fatigue. In this two-dimensional frame, the Chevron brace is connected to the TADAS damper and the TADAS damper is simulated with two node link elements.

Table 1. Geometry and Details of Frame Sections.

| Story Number Story		Exterior Columns	Interior Columns	Bracing Element	Beams
3 Story 9/1 Span	1,2,3	W12×22, W12×19, W12×16	W14×26, W14×22, W12×16	UPA100, UPA80, UPA80	W14×30, W14×30, W12×26
6 Story 9/1 Span	1,2,3	W16×31, W14×26, W14×26	W14×34, W16×36, W16×31	UPA240, UPA180, UPA160	W14×30, W14×30, W14×30
	4,5,6	W14×22, W10×19, W12×19	W14×26, W14×22, W12×19	UPA140, UPA100, UPA80	W16×36, W14×30, W12×22
9 Story 9/1 Span	1,2,3	W18×55, W18×35, W18×35	W18×60, W18×40, W18×40	UPA240, UPA180, UPA160	W14×34, W14×34, W14×30
	4,5,6	W18×35, W14×26, W14×26	W18×40, W14×30, W14×26	UPA160, UPA160, UPA120	W14×30, W14×30, W14×30
	7,8,9	W14×22, W12×19, W12×19	W14×26, W14×22, W12×16	UPA100, UPA80, UPA80	W14×30, W14×30, W14×31
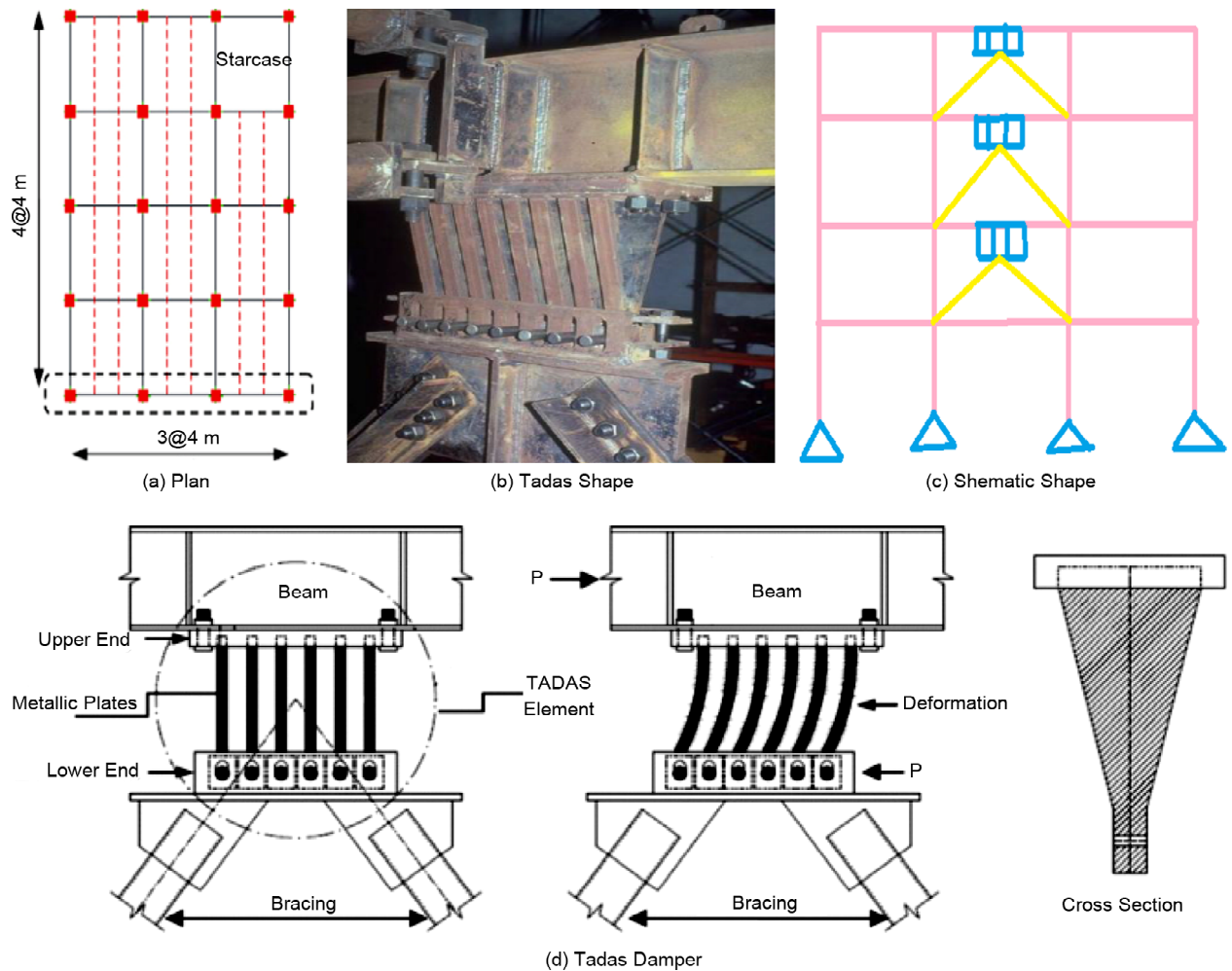
Figure 2. The Placement of TADAS damper in the structure.

Two node link elements show nonlinear shear behavior as well as nonlinear bending behavior. The equal DOF command is used to simulate the rigid behavior of the roof. Newmark method with $\alpha = 0.5$ and $\beta = 0.25$ parameters and Rayleigh damping principle with 5% damping ratio was used in dynamic analysis.

4. Applied Accelerographs

In this section, 10 earthquake records in FEMA P695 regulations (2009) have been used for incremental dynamic analysis of the studied models. The specifications of the applied records are given in Table (2).

The models studied in this paper, including three 3, 6 and 9-story frames, were studied with the TADAS eccentrically brace steel frame system and with 9.1 span. These frames have been extracted from each of the two-dimensional models for incremental dynamic analysis and

Table 2. Specifications of earthquake records used in incremental dynamic analysis of models.

Number	Record of Earthquake	PGA
1	Kocaeli	0.36
2	Impvall	0.38
3	Landers	0.42
4	Northridge	0.48
5	Kobe	0.51
6	Manjil	0.51
7	North Palm Springs	0.52
8	Lomap	0.53
9	Northridge	0.56
10	Duzce	0.82

simulated in OpenSEES software.

Performance levels or limit conditions are the basic principles in performance-based earthquake engineering, and the IDA curve has the necessary information to achieve this. Therefore, in order to use this information, it is first necessary to find accurate and quantitative criteria for different performance levels; therefore, it is necessary to

determine how much of each of different performance levels corresponds to the criterion of collapse intensity (maximum ratio of relative inter-floor displacement in this study). Consequently, the failure criterion was determined according to HAZUS regulations (2012).

5. IDA Curves Obtained from Incremental Dynamic Analysis of the Studied Frames

In this section, the IDA curves obtained from the incremental dynamic analysis of the three frames studied are presented in Figures (3) to (5) under 10 seismic records listed in Table (2). Looking at
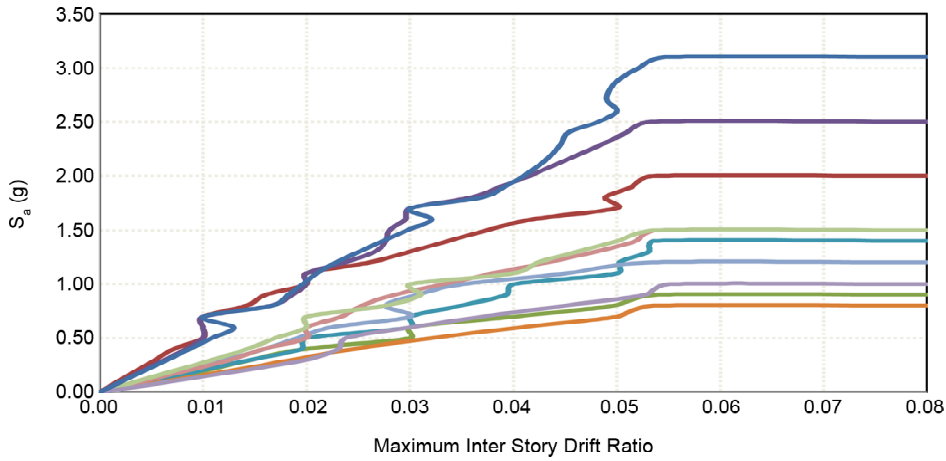
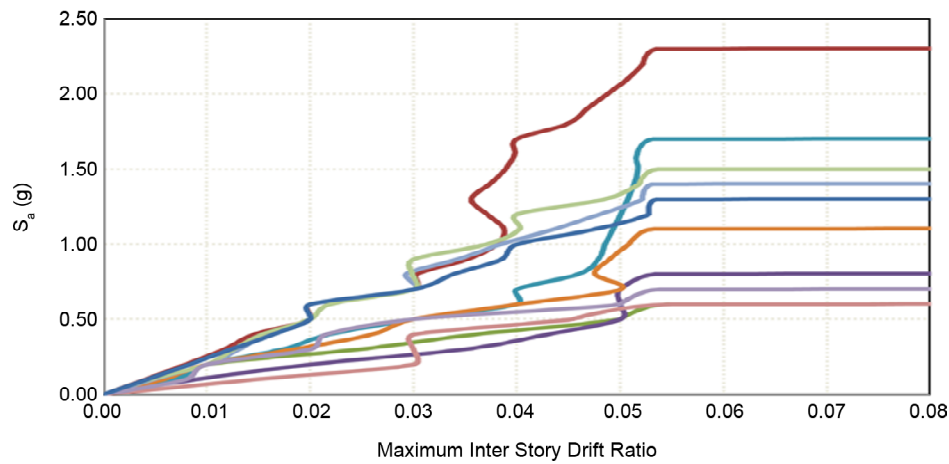**Figure 4.** IDA curves for 3-story frames.
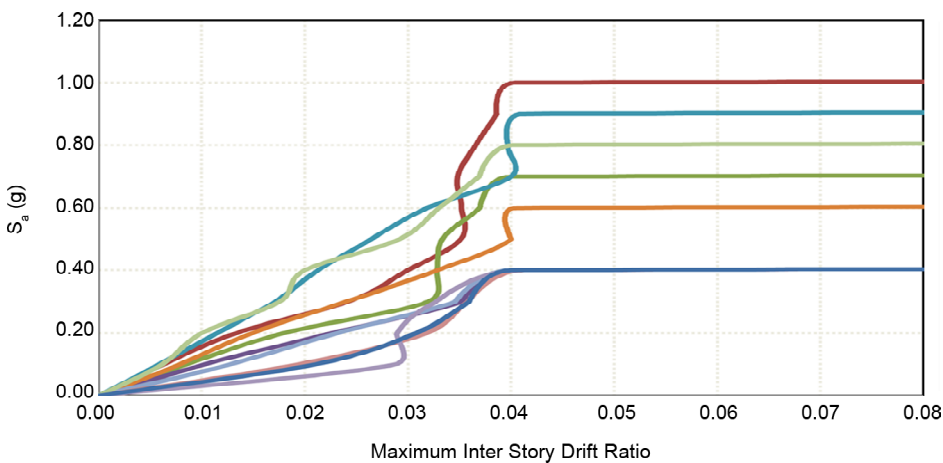
Figure 4. IDA curves for 6-story frames.

Figure 5. IDA curves for 9-story frames.

IDA curves, we can observe all the phases of structure behavior under the earthquake, from the reactionary level to the collapse and overall instability. At the beginning of all the curves there is an elastic area that is in the form of a straight line and it is common in all the curves. After this area, the nonlinear behavior in the curves is shown by the departure of the curve from the smooth line state, and by decreasing or increasing hardness, the nonlinear behavior of the structure is shown. Therefore, by looking at the IDA curves, we can get an overview of the frame behavior, from full elastic to complete failure. Comparing the behavior of frames with different heights, it can be said that with increasing height, the structures enter the nonlinear area earlier and have less capacity.

5. Summarizing IDA Curves

After performing IDA analysis under several different earthquake records, a class of IDA curves is obtained, which due to the large number of diagrams in a curve group, each of which rep-resents a specific behavior of the structure under earthquake records and does not express the overall performance of the structure in all types of earth-quake. In order to achieve a general state of structural behavior and reduce the scattering of information, IDA curves can be summarized. This is possible through statistical methods, and thus the capacity of the studied buildings can be evaluated. Therefore, in this section, three statistical values of 16%, 50% and 84% of each IDA curve have been extracted and they have been used to compare different curves with each other and probabilistic evaluation of structures. Each of the summarized curve classes are shown by the statistical figures mentioned in Figures (6) to (8).

As shown in Figures (6) to (8), as the building height increases the IM values decrease in the graphs for a constant value of DM. Also, the mean value of Sa corresponding to the limit state of collapsing in IDA curve is called the Sa capacity of structures. Given the average curves of these figures, it can be said that the Sa capacity of structures decreases as the height increases.

Also, looking at the not summarized IDA curves, it is observed that reaching the limit state of collapse (HAZUS, 2012) accompanies with more

severe softening in the behavior curve in 6 and 9 story frames than in 3 story frames. While this softening is hardly visible in the behavior of the 3 story frame.
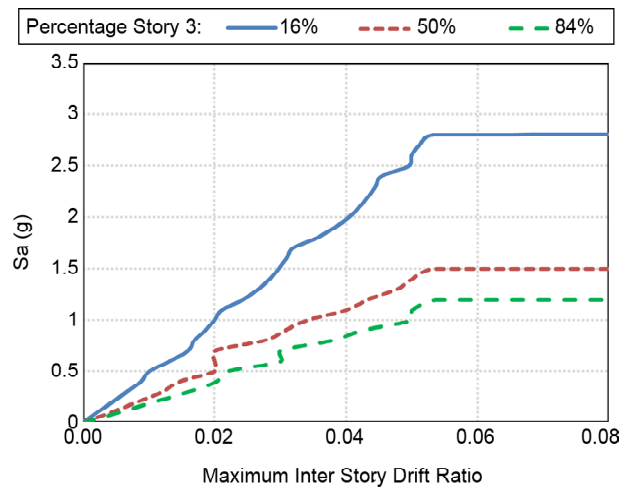

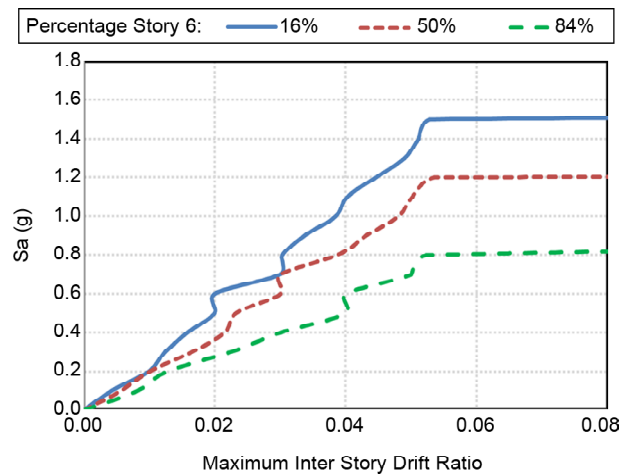**Figure 6.** Summarized IDA curves for simulated 3-story frame.

Figure 7. Summarized IDA curves for simulated 6-story frame.
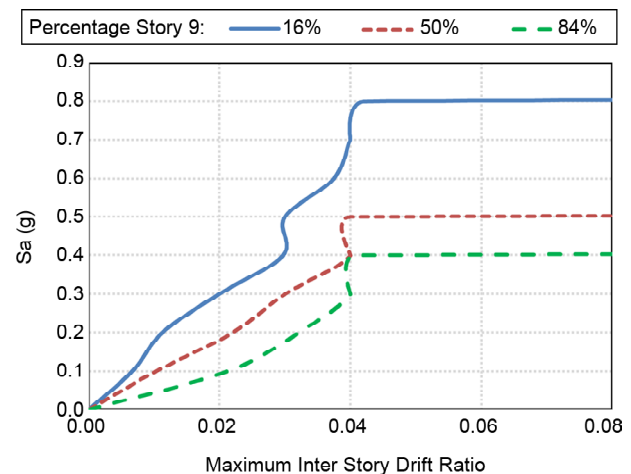

Figure 8. Summarized IDA curves for simulated 9-story frame.

6. Estimating the Probability of the Limit State Occurrence

In order to extract the probability of limit states occurrence from IDA analysis outputs, the fragility curves are used. To draw these graphs, first the IM values corresponding to the desired limit state are arranged in descending order for all records. Then, using the sorted values, the probability of occurrence of a limit state in the structure is calculated for smaller or equal amounts of a given IM value, which is a Cumulative Distribution Function, and its graph is plotted against IM.

Using this graph, it is possible to determine the probability of occurrence of a limit state at each functional level of the structure and for each IM level, without considering the seismic hazard, provided that the intensity level is limited to the desired level.

Figures (9) to (11) show the fragility curves of the structures, taking into account two limit states of continuous operation, IO and collapse threshold, CP. Also, the calculations for the fragility curves of the structures corresponding to the IO and CP levels are given in Tables (3) to (8).
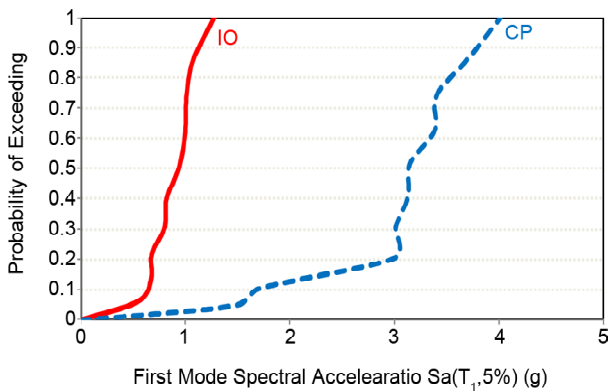

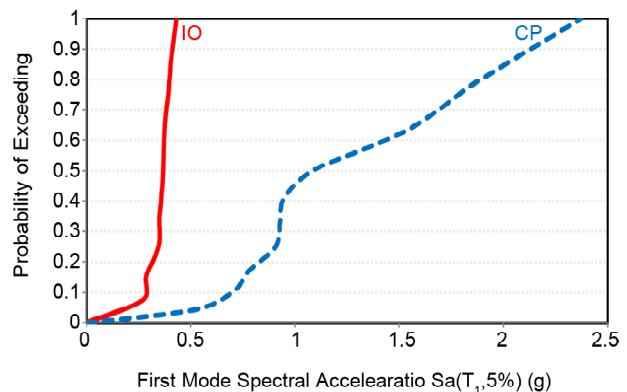**Figure 9.** Fragility curve of a simulated 3-story frame.

Figure 10. Fragility curves of a simulated 6-story frame.
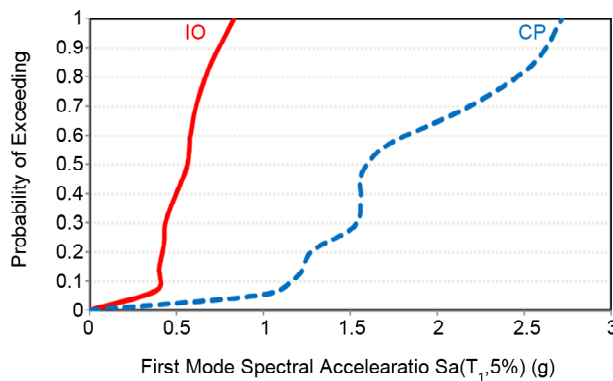
Figure 11. Fragility curves of a simulated 9-story frame.

Table 3. Calculating the values of the cumulative probability of failure for a 3-story structure at the IO functional level.

Record	$S_a(T_1,5\%)$, DM=2% Corresponding	Sorted $S_a(T_1, 5\%)$	Cumulative Values $S_a(T_1, 5\%)$	Cumulative Probability $S_a(T_1, 5\%)$
1	0.577	0.573	0.573	0.053
2	0.702	0.577	1.15	0.150
3	0.820	0.667	1.82	0.226
4	0.843	0.702	2.52	0.327
5	0.98	0.820	3.34	0.432
6	1.003	0.843	4.18	0.522
7	0.667	0.98	5.16	0.621
8	0.573	1.003	6.17	0.726
9	1.28	1.08	7.25	0.841
10	1.08	1.28	8.53	1

Table 4. Calculating the cumulative probability of failure for a 3-story structure at CP operating level.

Record	$S_a(T_1,5\%)$, DM=2% Corresponding	Sorted $S_a (T_1, 5\%)$	Cumulative Values $S_a (T_1, 5\%)$	Cumulative Probability $S_a (T_1, 5\%)$
1	1.325	1.325	1.325	0.0323
2	2.28	1.63	2.96	0.116
3	3.129	2.28	5.24	0.227
4	3.806	3.01	8.25	0.343
5	3.4	3.02	11.25	0.422
6	3.35	3.129	14.39	0.526
7	3.26	3.26	17.65	0.649
8	1.63	3.35	21	0.753
9	3.01	32.4	24.40	0.843
10	3.02	3.806	28.21	1

Table 5. Calculating the cumulative probability of failure for a 6-story structure at the IO functional level.

Record	$S_a(T_1,5\%)$, DM=2% Corresponding	Sorted $S_a (T_1, 5\%)$	Cumulative Values $S_a (T_1, 5\%)$	Cumulative Probability $S_a (T_1, 5\%)$
1	0.701	0.110	0.11	0.02
2	0.634	0.202	0.31	0.11
3	0.522	0.221	0.53	0.223
4	0.343	0.321	0.85	0.454
5	0.409	0.343	1.20	0.449
6	0.453	0.409	1.61	0.501
7	0.321	0.453	2.06	0.622
8	0.221	0.522	2.58	0.705
9	0.201	0.634	3.22	0.866
10	0.110	0.701	3.92	1

Table 6. Calculating the cumulative probability of failure for a 6-story structure at CP operating level.

Record	$S_a(T_1,5\%)$, DM=2% Corresponding	Sorted $S_a (T_1, 5\%)$	Cumulative Values $S_a (T_1, 5\%)$	Cumulative Probability $S_a (T_1, 5\%)$
1	2.23	0.57	0.57	0.12
2	1.53	0.602	1.17	0.145
3	1.50	0.732	1.90	0.173
4	1.43	0.843	2.75	0.243
5	0.732	1.02	3.77	0.333
6	0.843	1.3	5.07	0.453
7	1.02	1.43	6.5	0.523
8	1.3	1.50	8.00	0.626
9	0.602	1.53	9.53	0.723
10	0.57	2.23	11.76	1

Table 7. Calculating the values of the cumulative probability of failure for a 9-story structure at the IO functional level.

Record	$S_a(T_1,5\%)$, DM=2% Corresponding	Sorted $S_a (T_1, 5\%)$	Cumulative Values $S_a (T_1, 5\%)$	Cumulative Probability $S_a (T_1, 5\%)$
1	0.432	0.123	0.123	0.03
2	0.123	0.145	0.27	0.123
3	0.233	0.19	0.46	0.243
4	0.243	0.20	0.66	0.333
5	0.339	0.201	0.86	0.376
6	0.201	0.229	1.09	0.425
7	0.145	0.233	1.32	0.635
8	0.209	0.243	1.56	0.701
9	0.20	0.339	1.90	0.826
10	0.19	0.432	2.34	1

Table 8. Calculating the values of cumulative probability of failure for a 9-story structure at CP operating level.

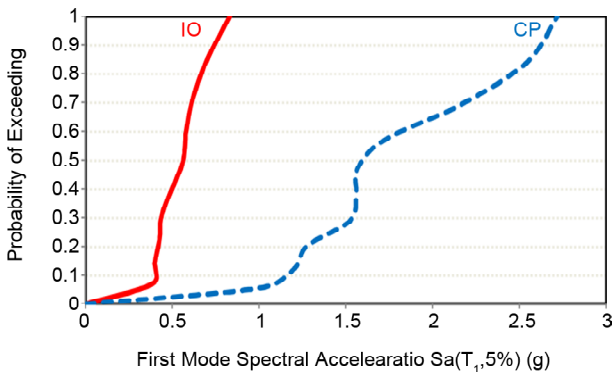| Record	$S_a(T_1, 5\%)$, DM=2% Corresponding	Sorted $S_a(T_1, 5\%)$	Cumulative Values $S_a(T_1, 5\%)$	Cumulative Probability $S_a(T_1, 5\%)$
1	1.001	0.40	0.40	0.042
2	0.40	0.41	0.81	0.051
3	0.60	0.60	1.41	0.129
4	0.61	0.61	2.02	0.297
5	0.65	0.65	2.67	0.345
6	0.83	0.76	3.43	0.428
7	0.85	0.80	4.23	0.501
8	0.76	0.83	5.06	0.63
9	0.41	0.85	5.91	0.805
10	0.80	1.00	6.91	1

Figures (12) and (13) compare the fragility curves of the limit states of collapse and the immediate ability to use them for all three structures under study, and the corresponding Sa values of 16%, 50%, and 84% failures for the two functional levels of continuous operation, IO and collapse threshold, CP are presented in Table (9). The values of Sa corresponding to the probability of a 50% collapse, called the Sa capacity of the structure, are given in Table (10).

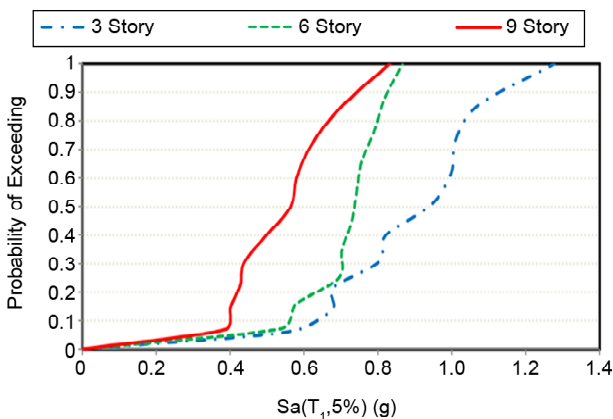**Table 9.** S_a values corresponding to different occurrence probabilities.

Story	$(S_a(T_1,5\%))_{IO}$ (g)			$(S_a(T_1,5\%))_{CP}$ (g)		
	16%	50%	84%	16%	50%	84%
3	0.623	0.945	1.07	2.21	2.61	2.91
6	0.520	0.632	0.921	0.94	1.21	1.39
9	0.20	0.321	0.404	0.53	0.62	0.79

Table 10. S_a capacity of the studied structures.

Number of Stories	3	6	9
S_a Capacity of the Structure	2.81	1.32	0.75

By observing the figures and values in Tables (9) and (10), we see that as the height of the structures increases, the probability of collapse or failure to meet the IO performance level at a constant level of seismic intensity increases. The values in Table (9) can be used to determine the designed earthquakes with a certain probability of collapse or to assess the adequacy of structural design regulations against earthquake loads.

7. Distribution of Floor Drift at the Height of the Structure

To investigate the distribution of floor drift at the height of the structure, the mean values of maximum floor drift at certain levels of seismic intensity have been extracted and shown for all three buildings in Figures (14) to (16). These levels are the seismic intensities corresponding to the probabilities of collapse of 16%, 50% and 84%, which are extracted from the fragility curves for each structure, and then at these levels of seismic intensity, the time history analysis is performed and the maximum value of drifts are determined for each floor. As can be seen in the figures, drift accumulation in certain floors of the structure is the main cause of

Figure 12. Fragility curves of 3, 6 and 9-story structures at IO performance level.

Figure 13. Fragility curves of 3, 6 and 9-story structures at CP performance level.

structural failure and collapse. In fact, as the height of the building increases, the failure mode of the structure is associated with the increasing accumulation of drift in certain floors and while other floors have very little drift. This failure mode, which occurs due to the second order effects on the deformation of the structure, is called soft floor formation.
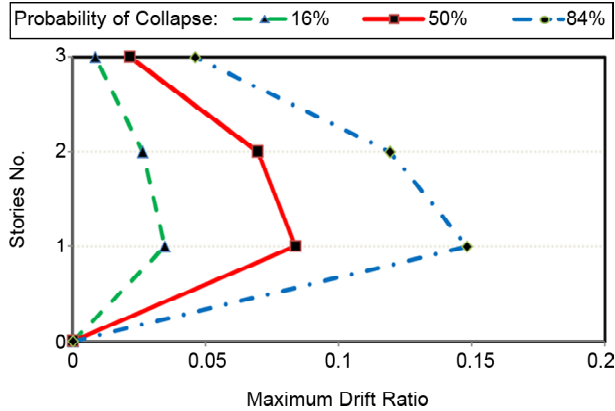

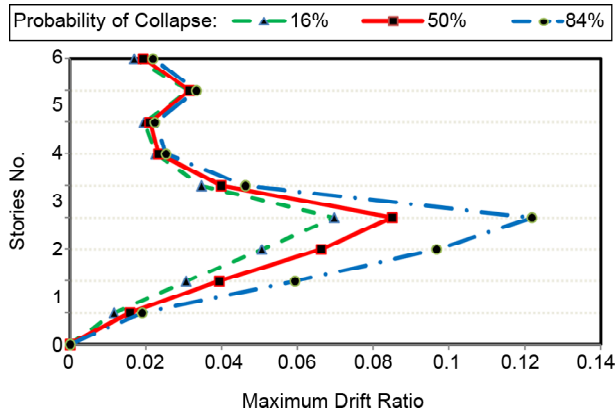**Figure 14.** Drift distribution at 3-story frame height at CP operating level.

Figure 15. Drift distribution at 6-story frame height at CP operating level.
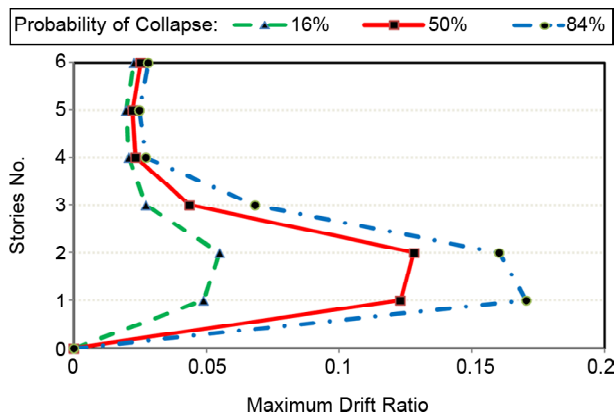

Figure 16. Drift distribution at 9-story frame height at CP operating level.

8. Probabilistic Seismic Demand Analysis (PSDA)

Probabilistic Seismic Demand Analysis is a method for calculating the mean annual frequency of structural seismic demand. In other words, probabilistic seismic demand analysis incorporates the seismic hazard curve (such as the spectral acceleration hazard curve) of the structure site calculated by PSHA, with the results of non-linear dynamic analysis of the structure under study, under the influence of a group of earthquake accelerograms. This method is an application of the general probability theory that is also the basis of the PSHA method. If *DM* represents the structural demand and *IM* represents the seismic intensity, the probabilistic seismic demand analysis is expressed as in Equation (1):

$$\lambda_{DM}(y) = \int G_{DM|IM}(y|x).\left|d\lambda_{IM}(x)\right| \qquad (1)$$

where $\lambda_{DM}(y)$ implies the mean annual frequency of *DM* exceeding the value of *y* (MAF), $\lambda_{IM}(x)$ is the value of the seismic hazard function in terms of IM at point x, and   is the differential of this function at this point. In other words, $d\lambda_{IM}(x)$ is the annual probability of specific earthquake intensity. The term, $\int G_{DM|IM}(y|x)$ which is usually calculated using nonlinear dynamic analysis results under a series of seismic accelerograms, indicates the probability of *DM* exceeding the value of *y* provided that *IM* is equal to *x*, also this term includes the uncertainty of structural demand at a level, especially from the severity of the earthquake that is caused by the difference in earthquakes. Also, the results of probabilistic seismic demand analysis can be used to calculate the mean annual frequency exceeding a certain limit state, which is usually indicated by λ_{LS}. λ_{LS} is calculated by Equation (2):

$$\lambda_{LS} = \int G_{LS|DM}(y).\left|d\lambda_{DM}(y)\right| \qquad (2)$$

$d\lambda_{DM}(y)$ shows the differential of seismic demand risk for *DM*, which means that the term determines the annual probability of a certain amount of *DM*. $\int G_{LS|DM}(y)$ provides the probable exceeding from *LS* limit state provided that *Dm* is equal to *y*.

A seismic demand curve λ_{DM}, or annual threshold frequency λ_{LS} calculated by Equations (1) or (2)

can be used in a design (or estimate) process based on the performance, for example, can be used to make decisions about the adequacy of a structural design or the need of an existing structure to be reinforced.

In order to calculate the mean annual frequency of the limit state, Equation (3) is obtained by expanding Equation (2).

$$\lambda_{LS} = \int_{IM=0}^{IM=\infty} F(IM^C|IM) \cdot \left|\frac{d\lambda_{IM}}{dIM}\right| dIM \qquad (3)$$

The expression within the absolute value is the gradient of *IM* risk and $F(IM^C|IM)$ is a cumulative probability function of a limit state occurrence according to the *IM* variable. The above relationship is the basis for calculating the limit states mean annual frequency. To calculate λ_{LS}, it is first necessary to obtain a diagram of the probability function $F(IM^C|IM)$ which is the same as the fragility curve and was drawn above for different limit states. After calculating the values of this curve, having the numerical values of the seismic hazard chart of the study area, the above integral can be easily calculated.

9. Seismic Hazard Curve

In order to calculate the seismic hazard gradient expression, $\left|\frac{d\lambda_{IM}}{dIM}\right|$, it is necessary to analyze the seismic hazard of the given structure. By conducting seismic hazard analysis for different parts of an area, simplified uniform hazard spectra are obtained with a return period of 475 and 2475 years. Then, according to the time of the main frequency of the structure, the spectral accelerations corresponding to the return period of 475 years and 2475 years can be determined. The annual frequency of seismic intensity (spectral acceleration in this study) is usually estimated by a linear relationship in the logarithmic space, which is as follows:

$$\lambda_{Sa} = k_0 (Sa)^{-k} \qquad (4)$$

In this relation, λ_{Sa} equals the reverse of the return period of the earthquake and S_a is the spectrum acceleration corresponds to the simplified uniform spectrum of hazards of 475 years and 2475 years. Also, the *k* parameter is the slope of

the seismic hazard curve in the desired capacity value and k_0 indicates the coefficient that is related to the shape of the seismic hazard curve. These two parameters can be calculated by having a seismic hazard curve or a uniformly simplified risk spectrum of the area with return periods of 475 years and 2475 years (Hazus, 2012). In this study, in order to evaluate the probability of seismic demand of the studied models, a simplified uniform risk spectrum was used for Tajrish region in the north of Tehran, which has latitude of 35.8 and a longitude of 51.42. The simplified uniform risk spectrum for this area is shown in Figure (17).
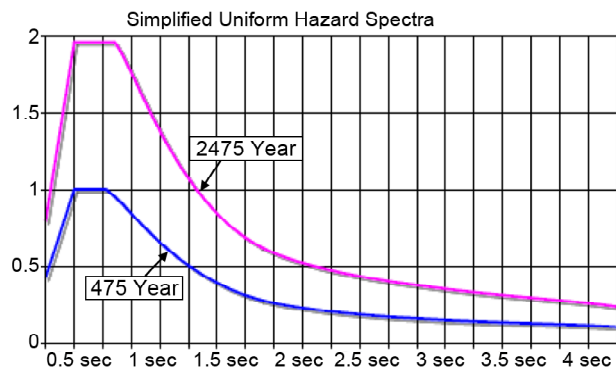

Figure 17. Simplified uniform risk spectra for geographical coordinates (35.8 and 51.42) in Tehran.

Table 11. Parameters for seismic hazard curves.

Number of Stories	3	6	9
Period (sec)	0.77	1.40	2.05
K	2.1803	2.1511	2.0853
K_0	1.18E-03	5.93E-04	4.43E-04

Also, the *k* and k_0 parameters related to the seismic hazard curve have been calculated using the uniformly simplified risk spectra and are given in Table (11).

10. Determining the Mean Annual Frequency of Limit States

By having simplified uniform risk spectra as well as the fragility curves shown in Section 6, numerical integration can be performed to calculate the mean annual frequency of limit states using Equation (3). The MAF values for the IO and CP limit states obtained from this integration are presented for all three structures studied in Tables (12) and (13), also for each return period

Table 12. Mean annual frequency of IO limit state.

Number of Stories	MAF	T_r (Year)	The Probability of Occurrence in 50 Years (%)
3	0.001753	523	8.88
6	0.000101	1120	4.32
9	0.001381	635	7.21

Table 13. Mean annual frequency of CP limit state.

Number of Stories	MAF	T_r (Year)	The Probability of Occurrence in 50 Years (%)
3	0.000132	8054	0.71
6	0.000152	7081	0.79
9	0.000141	6831	0.81

structure, T_r, the earthquake associated with the occurrence of limit states equal to the inverse of the MAF value, and the probability of a one-time occurrence of this earthquake has been calculated during 50 years and 2800 Standard has been presented to compare with the basic design earthquake, and maximum probable earthquake.

In order to calculate the probability of an earthquake occurring during the 50 years of useful life of the structure, the distribution of Poisson's probability has been used according to Equation (5). The Poisson distribution is a discrete probability distribution that describes the probability that an accident will occur in a certain number of times in a time interval or at a fixed location, provided that these events occur at a certain average rate and independent of the time of the last accident. According to Poisson's probability distribution, if the mathematical expectation of the occurrence of an event is in a given interval λ, the probability that we have exactly *k* emergence (*k* is an incorrect integer) equals to:

$$P(k,\lambda) = \frac{\lambda^k e^{-\lambda}}{k!} \tag{5}$$

These values can be used to measure the structural reliability of buildings in comparison with other structures or they can be used in the regulations of the design of buildings under consideration. As can be seen from the values, although without considering the seismic hazard values in calculating the probability of structural failure, according to Figure (5), the probability of the failure increases as the number of stories increases, but after incorporating the above results with seismic hazard

values, the result is reversed. In other words, the overall probability of the failure of taller structures is lower. This is because of the fact that the effect of increasing the frequency time of structures on the reduction of the simplified uniform risk spectra, according to Equation (4), neutralizes the increased probability of exceeding a certain functional level resulting from the increase in height of the structure.

Also, considering the probability calculated for an earthquake corresponding to limit states, it is observed that the probability of an earthquake corresponding to IO limit state in 50 years of useful life of the structure is less than the probability of Standard 2800 (BHRC, 2008) earthquake with a return period of 475 years, which is 10% in 50 years. Also, the probability of an earthquake corresponding to the CP limit in 50 years of useful life of the structure in all cases is less than the probability of Standard 2800 maximum possible earthquake and instructions for improvement of existing buildings (MPORG, 2007), with a return period of 2475 years which is 2% in 50 years. This indicates that the design of steel frames with a gate restraint system with appropriate behavior factor and resistance factor using Standard 2800 design has sufficient reliability in short and medium buildings.

11. Seismic Demand Hazard Curve

The output of the probability seismic demand analysis is typically the curves that derive the limit state annual frequency of the structure from the various limit states, which is given in section 8 (Equation 3). In this relation, if, instead of the limit state, exceeding a certain level of demand is considered, by using this relationship simultaneously with the seismic risk curve, the seismic demand curves of the structures are obtained. These curves are obtained using the same method using Equation (3) and the calculation of mean annual frequency from different values of the maximum relative lateral displacement ratio of the structure is obtained for the TADAS damper system and is shown in Figure (18).

As noted above, although the probability of a particular demand occurring at a given risk level is higher for taller structures (Figures 12 to 13), given the seismic risk curve, the overall probability of a particular demand reduces in taller structures.
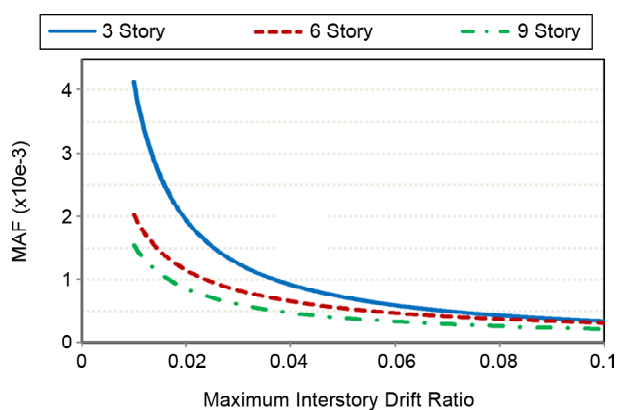
Figure 18. Seismic demand hazard curves for the TADAS damper system.

12. Conclusions

In this study, a TADAS damper connection model was created and validated based on laboratory results and limited components, which reflected its behavior well. Subsequently, the curved frames modeled using these connections were analyzed by IDA. With the help of the seismic demand probability analysis, the performance of the frames was expressed in the form of "limit state frequency", "seismic demand curve of structures".

The distribution of the maximum mean relative displacement in the stories was also estimated and studied using IDA analysis results.

The probability values associated with the occurrence of the two functional levels of IO and CP obtained for the studied frames can be a criterion for comparing the performance of different structures or can be used to estimate the adequacy of the regulations used in the design of frames. In addition, seismic demand curves obtained by the annual frequency from different levels of seismic demand can be used to estimate the performance of the studied frames. In addition to the above applications, comparisons between graphs related to different structures lead to the following results:

- Comparisons between fragility curves show that regardless of the probability distribution of seismic intensity values (seismic hazard curves), the probability of collapse (or exceeding the IO level) is higher in taller buildings.
- Despite the results of fragility curves, the comparison between seismic demand hazard curves indicates that the probability of failure increases as the number of floors increases,

without considering the seismic hazard values in calculating the probability of failure. However, after entering the seismic hazard values, the result is reversed. This means that the overall probability of failure of taller structures is lower. This is due to the fact that the effect of reducing the oscillation period of the structures on increasing the seismic hazard neutralizes the probability of exceeding a certain functional levels as a result of reducing the height of the structure.

- Graphs of median values of the maximum relative displacement between different stories at the seismic level corresponding to 84% probability of collapse, as well as the median IDA diagrams obtained for the frames, reveal the difference between the collapse behaviors of low and high-rise structures.

References

Ahmadi Amiri, H., Najafabadi, E.P. & Estekanchi, H.E. (2018). Experimental and analytical study of Block Slit Damper. *Journal of Constructional Steel Research, 141*, 167-178.

Apostolakis, G. & Dargush, G.F. (2010). Optimal seismic design of moment-resisting steel frames with hysteretic passive devices. *Earthquake Engineering and Structural Dynamics, 39*(4), 355-376. https://doi.org/10.1002/eqe.944.

Bayat, K. & Shekastehband, B. (2019). Seismic performance of beam to column connections with T-shaped slit dampers. *Thin-Walled Structures, 141*, 28-46, https://doi.org/10.1016/j.tws.2019.04.010.

Benavent-Climent, A. (2008). Development and application of passive structural control systems in the moderate-seismicity Mediterranean area: the case of Spain. *In Proceedings of the 14th World Conference on Earthquake Engineering*, Beijing, China.

BHRC (2008). I*ranian Code of Practice for Seismic Resistant Design of Buildings.* Standard No. 2800. 4th ed. Building and Housing Research Center, Tehran.

Chan, R.W. & Albermani, F. (2008). Experimental study of steel slit damper for passive energy dissipation. *Engineering Structures, 30*(4), 1058-

1066.

Chan, R.W., Yuen, J.K., Lee, E.W. & Arashpour, M. (2015). Application of Nonlinear-Autoregressive-Exogenous model to predict the hysteretic behaviour of passive control systems. *Engineering Structures, 85*, 1-10.

FEMA (2009). *FEMA P695*. Federal Emergency Management Agency, Washington, DC.

Gur, S., Xie, Y. & DesRoches, R. (2019). Seismic fragility analyses of steel building frames installed with superelastic shape memory alloy dampers: Comparison with yielding dampers. *Journal of Intelligent Material Systems and Structures, 30*(18-19), 2670-2687.

HAZUS (2012). *Hazus Multi-Hazard Loss Estimation Methodology, Earthquake Model, Hazus®-MH 2.1 Technical Manual.* Department of Homeland Security, Federal Emergency Management Agency, Mitigation Division, Washington, D.C., 718.

Karavasilis, T.L., Kerawala, S. & Hale, E. (2012). Hysteretic model for steel energy dissipation devices and evaluation of a minimal-damage seismic design approach for steel buildings. *Journal of Constructional Steel Research, 70*, 358-367, https://doi.org/10.1016/j.jcsr.2011.10.010.

Katal Mohseni, P., Zahedi-Khameneh, A. & Naeemifar, O. (2020). Study of the effect of geometric parameters of steel block slit dampers on energy absorption. *International Journal of Steel Structures*, 1-11. https://doi.org/10.1007/s13296-020-00343-3.

Keykhosravi, A. & Aghayari, R. (2017). Evaluating response modification factor (R) of reinforced concrete frames with chevron brace equipped with steel slit damper. *KSCE Journal of Civil Engineering, 21*(4), 1417-1423, https://doi.org/10.1007/s12205-016-1055-7.

Khatib, I.F., Mahin, S.A. & Pister, K.S. (1988). *Seismic Behavior of Concentrically Braced Steel Frames.* Earthquake Engineering Research Center, University of California.

Lee, C.H., Lho, S.H., Kim, D.H., Oh, J. & Ju, Y.K. (2016). Hourglass-shaped strip damper subjected to monotonic and cyclic loadings. *Engineering Structures, 119*, 122-134. https://doi.org/10.1016/j.engstruct.2016.04.019.

Lee, J., Kang, H. & Kim, J. (2017). Seismic performance of steel plate slit-friction hybrid dampers. *Journal of Constructional Steel Research, 136*, 128-139, https://doi.org/10.1016/j.jcsr.2017.05.005.

MPORG (2007). *Guidelines for Seismic Rehabilitation of Existing Buildings.* Management and Planning Organization. Publication No. 360, Iran.

Oh, S.H., Kim, Y.J. & Ryu, H.S. (2009). Seismic performance of steel structures with slit dampers. *Engineering Structures, 31*(9), 1997-2008, https://doi.org/10.1016/j.engstruct.2009.03.003.

Saffari, H., Hedayat, A.A. & Nejad, M.P. (2013). Post-Northridge connections with slit dampers to enhance strength and ductility. *Journal of Constructional Steel Research, 80*, 138-152, https://doi.org/10.1016/j.jcsr.2012.09.023.

Teruna, D. R., Majid, T. A. & Budiono, B. (2015). *Experimental Study of Hysteretic Steel Damper for Energy Dissipation Capacity.* Advances in Civil Engineering. https://doi.org/10.1155/2015/631726.

Tsai, K.C., Chen, H.W., Hong, C.P. & Su, Y.F. (1993). Design of steel triangular plate energy absorbers for seismic resistant construction. *Earthquake Spectra, 9*(3), 505-528, https://doi.org/10.1193/1.1585727.

Wada, A., Huang, Y.H., Yamada, T., Ono, Y., Sugiyama, S., Baba, M. & Miyabara, T. (1997). Actual size and real time speed tests for hysteretic steel damper. *Proceedings of Stessa*, Kyoto, Japan, 778-785.

Wijaya, H., Rajeev, P., Gad, E. & Amirsardari, A. (2019). Effect of hysteretic steel damper uncertainty on seismic performance of steel buildings. *Journal of Constructional Steel Research, 157*, 46-58, https://doi.org/10.1016/j.jcsr.2019.02.016.

Winters, C.W. & Constantinou, M.C. (1993). *Evaluation of Static and Response Spectrum*

Analysis Procedures of SEAOC/UBC for Seismic Isolated Structures.

Xu, Y.H., Li, A.Q., Zhou, X.D. & Sun, P. (2011). Shape optimization study of mild steel slit dampers. *Advanced Materials Research, 168*, 2434-2438, https://doi.org/10.4028/www.scientific.net/AMR. 168-170.2434.